Numerical study of the effects of urban heat island on the characteristic features of the sea breeze circulation

ABHIJIT SARKAR, R S SARASWAT* and A CHANDRASEKAR

Department of Physics and Meteorology, I.I.T, Kharagpur, 721 302, India
**email: rsarswat@phy.iitkgp.ernet.in*

A two-dimensional numerical model is employed to study the effect of the coastal urban heat island on the sea breeze front and the thermal internal boundary layer height. The temperature at the land surface is determined by solving an energy budget equation. The effect of the urban heat island is studied by varying the width of the region and its intensity. During the early afternoon, the presence of the urban heat island enhances the strength of convergence of the sea breeze front and also reduces its inland penetration. The presence of the urban heat island causes increased thermal internal boundary layer height. Larger urban width causes larger vertical velocity and higher thermal internal boundary layer. Stronger convergence and higher thermal internal boundary layer are also obtained in case of larger heat island intensity.

1. Introduction

Starting from Estoque (1961) and Fisher (1961), many investigators have carried out numerical studies of sea breeze circulation (Neumann and Mahrer 1974; Pielke 1974; Anthes 1978; Kondo and Gambo 1979; Lu and Turco 1994 etc.) and rural urban circulation (Atwater 1975; Vukovich *et al* 1976; Bennett and Saab 1982; Seaman *et al* 1989 etc.). Coastal areas are often considered suitable sites for industry for various reasons. The growth of industry and the consequent urbanization modify the prevailing meteorological conditions of the coastal area. Yoshikado (1992) studied the interaction of the heat island circulation induced by the coastal urban heat island and sea breeze circulation. Yoshikado (1992) considered a two-dimensional model where urban area was treated always warmer than the rural area and the rural surface temperature was either constant (referred as steady case) or it varied sinusoidally with time (unsteady case). Yoshikado's study demonstrated some important characteristics of the sea breeze in the presence of the urban heat island. The effect of the change of the heat island intensity on some aspects of the sea breeze circulation was also studied.

The rapid expansion of an industrialized urban area increases the horizontal extent of the urban heat island as well as its intensity. The above can be correctly represented in a model by increasing the urban width and the heat island intensity. Since sea breeze front (SBF) and thermal internal boundary layer (TIBL) play major roles in the transfer of pollutant and moisture, we study the effect of urban width and its intensity on the SBF and TIBL in this paper.

The numerical experiments mentioned in the present paper were performed to study the variation of TIBL height and SBF characteristics due to the change of the width of the urban area and the heat island intensity. First, an experiment was carried out without considering any urban area in the model domain (case 1). Then an urban area was considered on the coast (case 2). Comparative study of the results obtained from these two experiments gives the effect of the presence of the urban heat island (UHI) on the sea breeze characteristics mentioned above. In case 3 the effect of the variation of urban width and in case 4 the effect of variation of anthropogenic heat flux (which in turn, changes the heat island intensity) were studied. Section 2 provides a detailed discussion of the model used in the study while section 3 provides the

Keywords. Heat island circulation; urban heat island; Sea Breeze Front; Thermal Internal Boundary Layer.

Proc. Indian Acad. Sci. (Earth Planet. Sci.), **107**, No. 2, June 1998, pp. 127–137

results and discussion of this study. Section 4 summarizes the results of the paper.

2. Model description

2.1 *Model equations*

A two-dimensional mesoscale numerical model was used. The x-axis was taken horizontally and perpendicular to the shore and the z-axis in the vertical. The model domain was assumed to be flat. The basic model equations are the equations of momentum, equation of thermodynamic energy, hydrostatic equation and the continuity equation. The full model equations are not provided here as they are available in Xian and Pielke (1991), Yoshikado (1992) and many others. However, various quantities which appear in the basic model equations are defined in the Appendix. Vertical eddy exchange coefficients for momentum (K_z^m) and heat (K_z^h) were calculated from the formula proposed by Yamamoto (1975) and used by Kondo and Gambo (1979). Horizontal eddy exchange coefficients for momentum and heat were assumed to be constant and equal: $K_x^m = K_x^h = K_x = 20000\text{m}^2/\text{s}$.

The horizontal and vertical grid spacings were chosen to be uniform and they are 5 km and 50 m, respectively. The first 50 m above the lower boundary was considered to be the surface layer. The time step Δt was 60 seconds. The number of grid points along horizontal and vertical directions is 81 each.

The surface temperature at each time step is determined by solving the energy balance equation over the land surface, while the sea surface temperature is held constant.

With a slight modification in the values of c_1 and c_2, Deardorff (1978) has shown the superiority of Blackadar's (1978) model (referred as force-restore model) over the six other models to predict the surface temperature. This model has been used widely by Anthes and Warner (1978) and several others. We are using the Blackadar's model as modified by Deardorff (1978) to predict the surface temperature over land. In this model the ground temperature is predicted from the equation

$$\frac{\partial T_g}{\partial t} = \frac{c_1}{(\rho_s c_s)} \times \left(\frac{Q_S + Q_{LD} - Q_{LU} + Q_A - Q_{SEN} - Q_{LAT}}{(\kappa_s \tau_1)^{\frac{1}{2}}} \right) - \frac{c_2}{\tau_1}(T_g - T_d), \quad (1)$$

where

Q_S = Incoming short wave flux,

Q_{LD} = Downward long wave flux,

Q_{LU} = Upward long wave flux,

Q_A = Anthropogenic heat flux,

Q_{SEN} = Sensible heat flux,

Q_{LAT} = Latent heat flux.

The parameters used to solve the energy budget equation are also defined in the Appendix. (Blackadar used $c_1 = 3.72$ and $c_2 = 7.4$ whereas Deardorff considered $c_1 = 2\pi^{1/2}$ and $c_2 = 2\pi$.)

The solar radiative flux (Q_s) absorbed by the flat surface is given by

$$(t - a_f)(1 - A)S\cos Z, \quad (2)$$

where transmissivity (t), originally presented by Kondratyev (1969) and modified by Atwater and Brown (1974), is given by

$$t = 0.485 + 0.515 \times \left[1.041 - 0.16 \left(\frac{0.000949p + 0.051}{\cos Z} \right)^{1/2} \right], \quad (3)$$

where p is in hPa. In the present study p is assumed to have a value equal to 1000 hPa. a_f is the fractional absorption, A is the albedo, S is the solar radiation at the top of the atmosphere perpendicular to sun's ray and Z is the zenith angle.

$$S = S_0 \left[1 + 0.33 \cos \left(\frac{2n\pi}{365} \right) \right], \quad (4)$$

where S_0 is the solar constant and n is the julian day of the year.

Upward long wave radiative flux is computed from the equation

$$Q_{LU} = \epsilon_s \sigma T_g^4. \quad (5)$$

In our model, the surface emissivity (ϵ_s) has been taken to be unity, because radiation from most of the ground surfaces closely resembles a black body radiation (Pielke 1984).

The Long wave downward flux was determined according to Deardorff (1978)

$$Q_{LD} = [\sigma_c + (1 - \sigma_c)0.67(1670q_a)^{0.08}]\sigma T_g^4. \quad (6)$$

The cloud fraction (σ_c) has been chosen to be zero in this study.

Sensible heat flux is given by

$$Q_{SEN} = \rho c_p u_* \theta_*, \quad (7)$$

and the latent heat flux is given by

$$Q_{LAT} = \rho L_v u_* q_*. \quad (8)$$

u_*, θ_* and q_* are calculated at each time step by using Monin-Obukov's similarity theory in the surface layer. In the present model we have not used any prognostic equation for the specific humidity. The difference between the mixing ratio at the lower boundary and at the top of surface layer was assumed to be $0.20q_s$, where q_s is the saturation specific humidity

Table 1. *Summary of the numerical experiments.*

Experiment	Configuration	Urban width (km)	r_1 (Wm^{-2})	r_2 ($Wm^{-2}K^{-1}$)	T_m (^0K)
Case 1	Rural-sea	–	–	–	–
Case 2	Rural-urban-sea	20	50	250	293.0
Case 3(a)	Rural-urban-sea	10	50	250	293.0
Case 3(b)	Rural-urban-sea	30	50	250	293.0
Case 4(a)	Rural-urban-sea	20	30	200	292.5
Case 4(b)	Rural-urban-sea	20	70	300	294.0

corresponding to the lower boundary and is determined according to Pielke (1984).

For the anthropogenic heat flux over the urban area the expression proposed by Atwater (1975) is used

$$Q_A = \begin{cases} r_1 + r_2(T_m - T_g) & \text{if } T_g < T_m \\ r_1 & \text{if } T_g > T_m \end{cases}, \quad (9)$$

where r_1 and r_2 are constants for a given urban area. T_m is a temperature anticipated to be close to the minimum surface temperature of the urban region. Use of this formulation of Q_A ensures that the urban surface temperature does not go much below T_m. The values of r_1, r_2 and T_m considered for different cases in the present study are mentioned in table 1. Over the rural area Q_A is zero.

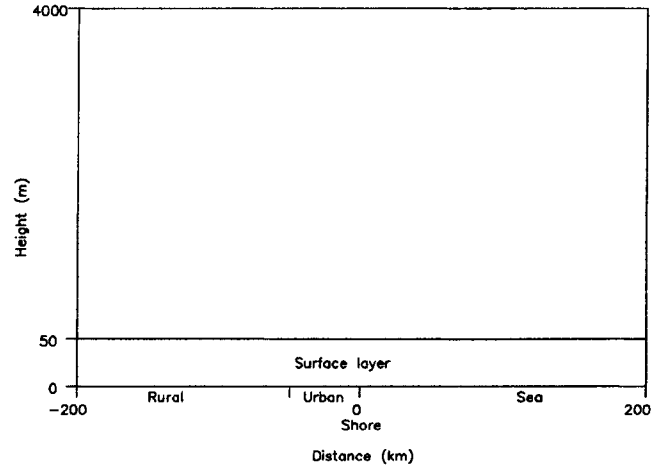

Figure 1. The configuration of the model domain.

2.2 *Initial and boundary conditions*

A stable lapse rate of $\Gamma = 0.004°K/m$ was prescribed for the initial potential temperature profile while the surface potential temperature (θ_{i0}) throughout the domain of the model was assigned a value of 300°K. The initial time was considered to be the time of sunset, 1800 Local Solar Time (LST). Completely calm atmosphere ($u = 0$, $v = 0$ and $w = 0$) was prescribed as the initial condition. In order to obtain the initialized input for the forecast, a procedure similar to that of Kondo and Gambo (1979) was employed in which low values of vertical eddy exchange coefficients ($K_z^m = K_z^h = 1.0\,m^2/s$) were chosen and the model was run for a duration of 12 hours. After this adjustment process, the model was integrated forward in time.

Roughness length of $z_0 = 0.001$ m over sea, 0.7 m over urban area and 0.05 m over rural area were considered in the present paper. Anthes (1978) used $z_0 = 0.00164$ m over the sea and $z_0 = 0.04$ m over the land. Kondo and Gambo (1979) and Feliks (1993) have used a value of 0.001 m for roughness length over the sea while Huang and Sethuraman (1988) used a value of 0.04 m for the roughness length over land. The roughness length of 0.7 m over the urban region has been taken from Pielke (1984). To avoid numerical difficulties, the roughness lengths of one suburban point (transition point between the rural and urban) and one coastal point (transition between urban and sea) were taken as the mean roughness lengths of the neighbouring points (Atwater 1975). At the lower boundary ($z = z_0$) $u = v = w = 0$. An 'open' condition at the lateral boundaries ($\partial(\theta, u, v)/\partial x) = 0$ was adopted in the model as was done by Mahrer and Pielke (1977); Anthes and Warner (1978) and several others. At the top of the model $u = v = 0$ and $\theta_H = \theta_{i0} + \Gamma H$, where H is the height of the model top. The Exner function, Π, at the top of the model was assumed constant.

The configuration of the model domain is shown in figure 1. The model equations were solved using finite difference methods which had **a)** upstream differencing for advection term, **b)** central differencing for horizontal diffusion terms and **c)** implicit differencing for vertical diffusion terms (Pielke 1984).

3. Model simulation, results and discussion

The model was integrated for a period of 28 hours after the adjustment process and we will confine our discussion to the period dominated by the sea breeze i.e., from 1200 LST to 2100 LST. The inland penetration of sea breeze front (SBF), the intensity of convergence and the height of thermal internal boundary layer (TIBL) were studied for different cases, listed in table 1. The position of SBF can be identified

Table 2. *Dependence of W_{max} and TIBL height on Γ for case 1.*

Γ (°K/m)	Max. TIBL height (m)	Max. TIBL height at x (km)	W_{max} (cm/s)	Max. W_{max} at x (km)	Max. W_{max} at z (m)	Time of Max. W_{max} (LST)
0.0030	2000	−30, −35	33.4	−55	1200	1600
0.0035	1850	−30, −35	24.7	−50	1100	1600
0.0040	1700	−30, −35	20.4	−50	1000	1600
0.0045	1600	−30	16.7	−50	900	1600
0.0050	1500	−30	13.8	−50	900	1600

by the location of the abnormally high gradient of several variables. Finkele *et al* (1995), in their study of sea breeze circulation cell from aircraft, considered the isolines of specific humidity and potential temperature to identify the SBF. In the same study Finkele *et al* also observed a strong upward vertical motion due to the convergence at the position of the front. In the present study the SBF was chosen to be the location of the domain maximum positive vertical velocity as suggested by Garratt and Physick (1985). The height of the TIBL was chosen as the height where the gradient of potential temperature profile, $\partial\theta/\partial z$, exceeds 1.0°K/km as was suggested by Anthes (1978). In all the figures, $x = 0$ denotes the shore while positive and negative values of x denote the area over sea and land, respectively. The values of the urban width considered for the different cases as well as the summary of the numerical experiments are mentioned in table 1.

In case 1, no urban region was considered in the model domain while in each of the other three cases an urban region near the coast was considered. The effect of urban width was studied in case 3 while the effect of heat island intensity was studied in case 4.

The main features of the sea breeze obtained from the model simulation for case 1 are in good agreement with various observational and modeling studies (Anthes 1978; Kondo and Gambo 1979; Garratt and Physick 1985; Arritt 1988; Zhong and Takle 1992 etc.). However, a quantitave comparison of the model results with previous modelling and observational studies cannot be carried out because of the differences in prevailing synoptic situations, locations of studies, characteristics of land surfaces, natures of the sea breeze generating thermal forcings assumed in different models, methods of boundary layer parameterization, numerical schemes, the horizontal and vertical resolution in various models etc.

The surface temperature near the coast is lower than that inland in the afternoon because of the penetration of cold sea breeze inside the land near the coast. The surface temperature at $x = -5$ km is 306.36°K and that at a point 80 km inland is found to be 309.26°K at 1400 LST. Model simulated surface temperature near the coast obtained by Kondo and Gambo (1979) was 2–3°K lower than the places inland in the afternoon. Anthes (1978) noted a temperature difference of over 4°K between the coast and a place 24 km inland 6 hours (the time of maximum heating) after the start of model simulation.

A maximum surface temperature of 307.59°K is noted to be at $x = -5$ km at 1230 LST, while a peak value of surface temperature of 309.26°K at $x = -80$ km is noted at 1400 LST. The numerical study of Kondo and Gambo (1979) showed that the maximum temperature peak appeared at 1200 LST at the coast, while that at the inland was at 1400 LST.

Maximum onshore component of sea breeze speed (5.59 m/s) and the inflow layer depth of 800 m at $x = -5$ km at 1400 LST obtained from the present model simulation agree well with those obtained by Anthes (1978) (5 m/s and 1.0 km, respectively at the time of maximum heating). The time of occurrence and the location of maximum onshore wind velocity simulated by the present model are also comparable with results tabulated by Kondo and Gambo (1979). Kondo and Gambo (1979) noted a maximum wind speed of 6.6 m/s at 36 km inland and 125 m above the surface at 1800 LST. The present model simulated maximum wind speed is 8.56 m/s at $x = -45$ km and $z = 200$ m at 1700 LST.

The study of the movement of the SBF obtained from the present model shows an acceleration of the front near sunset. The locations of the front noted at an interval of time of 1 hour from 1500 to 1900 LST are 35, 50, 70, 90 and 115 km inland, respectively. This feature agrees well with those observed by Garatt and Physick (1985); Physick (1980); and Kondo and Gambo (1979).

The offshore extent of sea breeze is nearly twice the onshore extent. The offshore extents noted at 1500, 1600 and 1700 LST (location of a minimum speed of 1.0 m/s is considered to be the limiting point of the extent) at a height of 150 m are 90, 120 and 150 km, respectively, while the onshore extents are 45, 60 and 80 km, respectively. Arritt (1988) showed from the three dimensional model simulation that the seaward extension of the sea breeze was about twice the landward extension. The observational study carried out by Zhong and Takle (1992) also shows a seaward extent of twice the landward extent.

To understand the effect of the prevailing synoptic situation considered as the initial condition, a sensitivity experiment has been performed by assuming

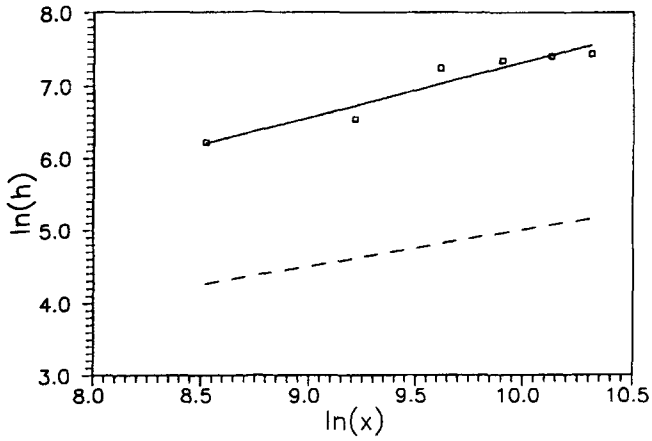

Figure 2. TIBL heights over land as a function of distance from the shore. The continuous line represents a best fit line for our model while the broken line represents a line with a slope of 0.5.

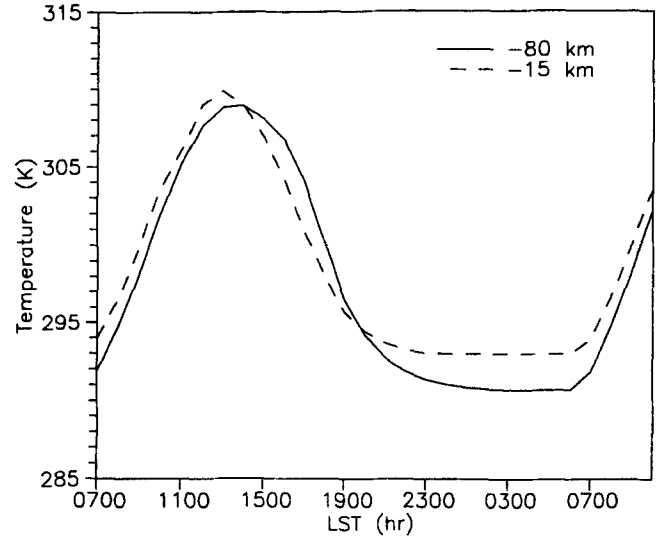

Figure 3. Diurnal surface temperature variation for case 2 at 15 km and 80 km inland.

different constant lapse rates as the intial condition. Table 2 shows that a prevailing stable atmosphere suppresses the TIBL. Although the magnitude and also the height of occurrence of the W_{max} decreases with the increase of the stability, there is no appreciable change in the time of occurrence and location in the horizontal direction of W_{max}.

Stunder and Sethuraman (1985) have compared observations of TIBL heights with six models and found that the observations compared very favourably with Weisman's (1976) formula. The TIBL height (h) over land according to Weisman's formula is given by

$$h = Px^{1/2},$$

where x is the distance from the shore and $P = (2q_h/\alpha c_p \rho u)^{1/2}$. q_h is surface heat flux, α is potential temperature gradient in the stable air mass and u is the mean wind speed. Weisman (1976) noted that the observations indicated the power of x varied from 0.37 to 0.67 with an average value of 0.50. Our results of the TIBL height over land (figure 2) indicate that the power of x (the distance from the shore) has a value close to 0.75.

3.1 *The effect of the presence of the urban area*

Figure 3 shows the diurnal surface temperature variation for case 2 at two different locations (one over urban area near coast while the other location is far inland in the rural area). It is clear from the figure that the surface temperature in the rural area reaches a maximum at 1400 LST while the cool sea breeze does not allow the urban surface temperature to increase after 1300 LST. The urban surface temperature is lower compared to the rural temperature during the afternoon and early evening hours. The above is attributed to the existence of sea breeze during the afternoon and early evening hours and to the proximity of the urban region to the sea. In the late night hours the urban surface temperature is much higher than the rural surface temperature.

Figures 4 and 5 show the distribution of u for case 1 and case 2, respectively at 1300 LST, 1500 LST and 1700 LST. At 1300 LST the speed of sea breeze in case 1 is maximum near the coast at a height of 200 m and its value is 4.6 m/s. The depth of sea breeze is the maximum height above which the reverse circulation from land to sea manifests. At 1300 LST the depth of sea breeze is observed to be 650 m near the coast (figure 4(a)). In case 2 the maximum speed of sea breeze is observed to be 5.4 m/s at this time. A rural urban circulation cell, which opposes sea breeze circulation, is also observed at 1300 LST (figure 5(a)). The maximum speed of this opposite flow is 0.3 m/s which occurs at 35 km inland. From figures 4(b) and 5(b) it is seen that both the speed and the depth of sea breeze have increased at 1500 LST for both case 1 and case 2. In case 1 the maximum magnitude of the sea breeze speed is 6.3 m/s and its depth near the coast is 800 m, whereas in case 2 the maximum magnitude and depth are observed to be 7 m/s and 850 m, respectively. The maximum speed of the rural-urban flow in case 2 is 0.4 m/s at 1500 LST. The rural-urban circulation is much weaker than the sea breeze circulation due to the smaller temperature differences at the surface for the former as compared to the latter.

Both the speed and the depth of sea breeze reach their maximum values for both the cases 1 and 2 (8.5 m/s and 900 m, respectively for case 1 and 7.9 m/s and 900 m, respectively for case 2) at 1700 LST (figures 4(c) and 5(c)). The maximum values of sea breeze speed occur at 45 km inland for case 1 and 35 km for case 2. However, at this time figure 5(c) does not show any reverse flow from rural to urban region.

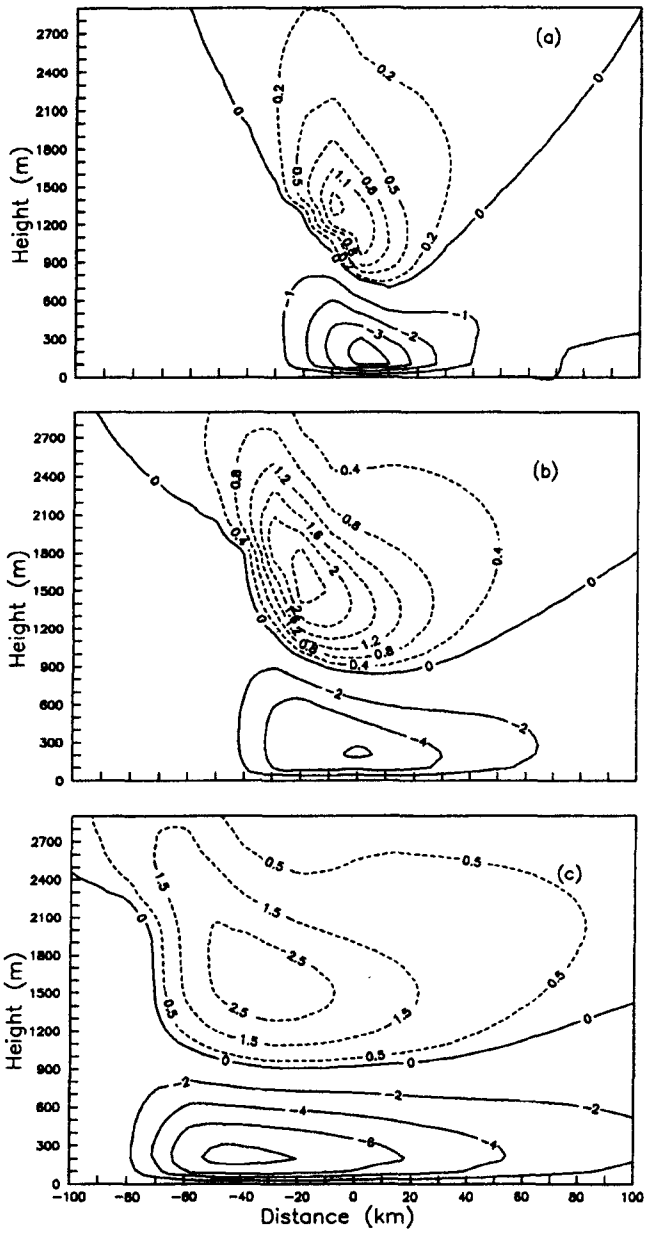

Figure 4. u in m/sec for case 1 at (a) 1300 LST, (b) 1500 LST, and (c) 1700 LST.

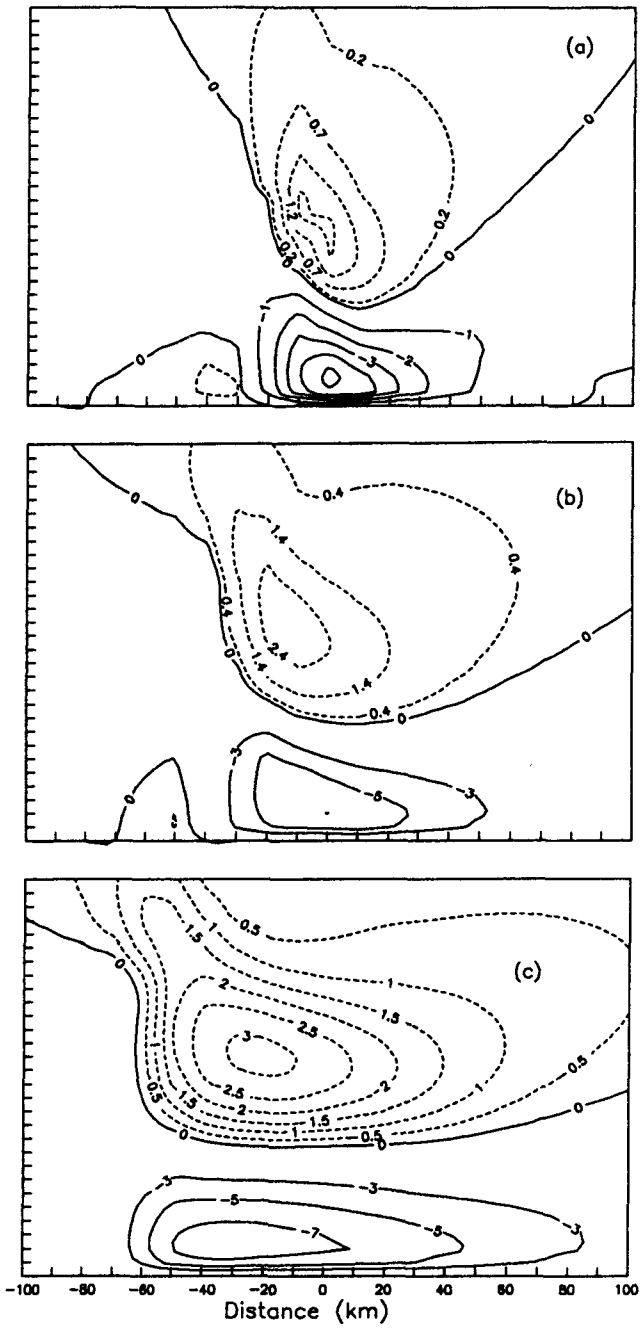

Figure 5. u in m/sec for case 2 at (a) 1300 LST. (b) 1500 LST, and (c) 1700 LST.

Figures 6 and 7 show the isolines of vertical velocity for case 1 and case 2 at 1300 LST, 1500 LST and 1700 LST. Maximum magnitudes of upward vertical velocity for case 1 are 8.6 cm/s (figure 6(a)), 16.1 cm/s (figure 6(b)) and 18.3 cm/s (figure 6(c)) at 1300 LST, 1500 LST and 1700 LST, respectively. A stronger vertical motion is observed in case 2 and the maximum magnitudes of upward vertical velocity are 15.3 cm/s (figure 7(a)), 23.5 cm/s (figure 7(b)) and 20.1 cm/s (figure 7(c)) at 1300, 1500 and 1700 LST, respectively. In case 2 subsidence of air is seen on both sides of the region of ascending motion. This is due to the convergence of the rural-urban circulation cell and sea breeze circulation cell. The subsidence in the rural-urban cell is strong at 1500 LST and the maximum magnitude of the downward vertical velocity in this rural-urban circulation cell is 1.78 cm/s at 60 km inland.

Figures 8(a) and (b) show the locations and magnitudes of maximum upward vertical velocity ($W_{\max}$) at different times for case 1 and case 2, respectively. In the afternoon hours values of $W_{\max}$ for case 2 are seen to be much higher than case 1. At 1400 LST the magnitude of $W_{\max}$ for case 1 is 12.3 cm/s (figure 8(a)) while for case 2 it is 20.8 cm/s (figure 8(b)). However, there are no appreciable differences in the evening hours (e.g., 9.7 cm/s for case 1 and 9.6 cm/s for case 2 at 2000 LST). In both the cases the magnitudes of vertical velocity become maximum at 1600 LST

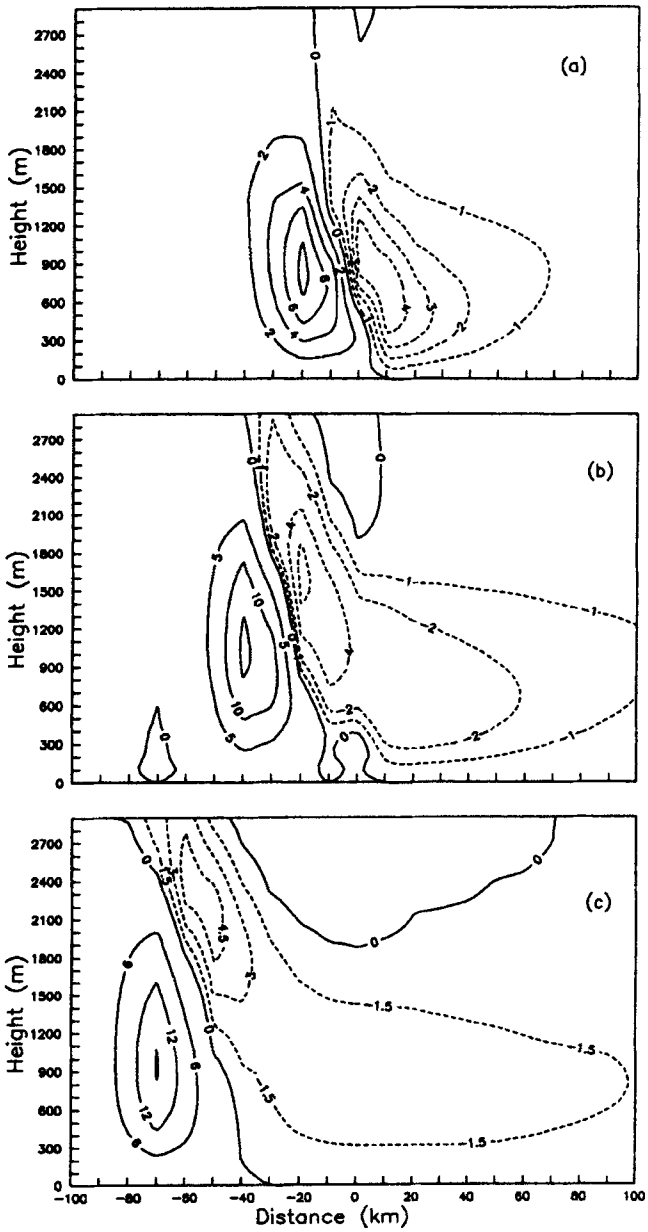

Figure 6. w in cm/sec for case 1 at (a) 1300 LST, (b) 1500 LST, and (c) 1700 LST.

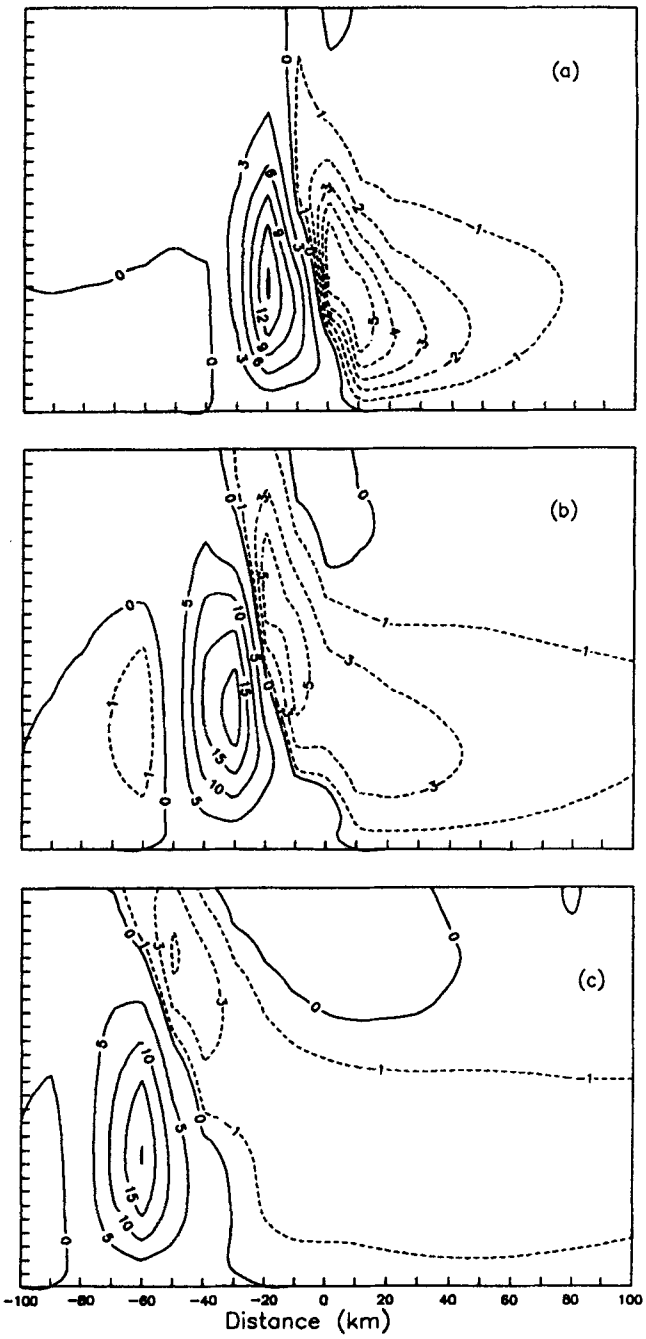

Figure 7. w in cm/sec for case 2 at (a) 1300 LST, (b) 1500 LST, and (c) 1700 LST.

(W_{max} = 20.4 cm/s for case 1 and 25.2 cm/s for case 2). The increased strength of convergence which yields higher W_{max} in case 2 during afternoon hours is partly due to the presence of the opposing rural-urban circulation cell and also due to the higher temperature contrast between the sea and urban surfaces. Figures 8(a) and (b) also reveal that during the time interval 1500 to 1700 LST the SBF for case 1 moves a distance of 35 km, while during the same time interval it moves 25 km for case 2. After 1700 LST the SBF for case 1 is always seen ahead of that for case 2 by a constant distance of 10 km. The SBF moves slower in case 2 during the time 1500 LST to 1700 LST due to the presence of the opposing rural-urban circulation cell.

Figure 9 shows the TIBL height at 1400 LST for cases 1 and 2. It shows that at 1400 LST the maximum values of TIBL height are 1700 m for case 1 and 1850 m for case 2. In both the cases the maxima occur above the location of W_{max} (30 km inland for case 1 and 25 km inland for case 2). The stronger heating over the urban area as well as the intense vertical motion in case 2 cause higher TIBL near the coast (by an amount of 150 m at 1400 LST).

3.2 *The effect of width of the urban area*

Figure 10 shows the locations of SBF and the magnitudes of W_{max} at different instants of time starting

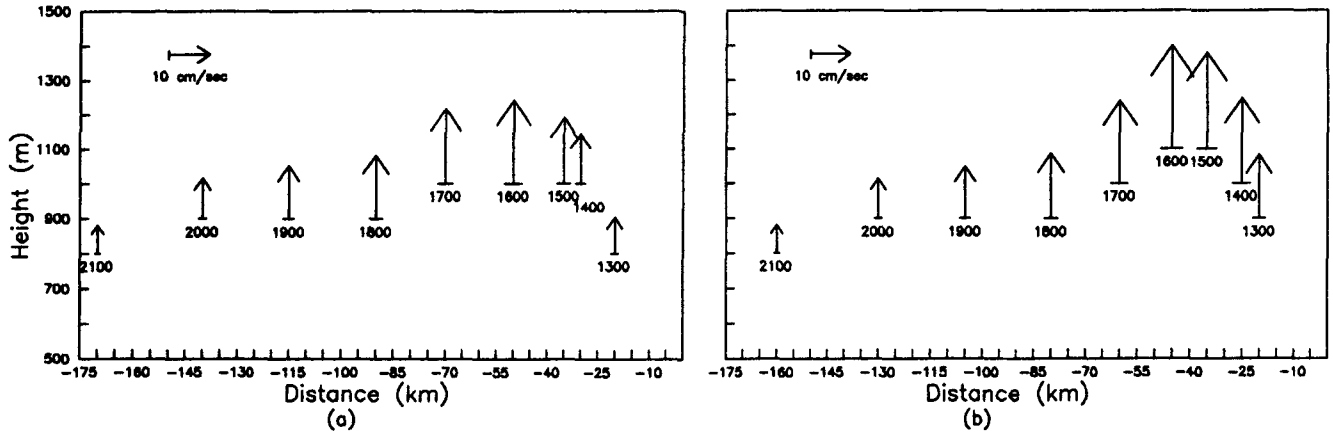

Figure 8. Locations and magnitudes of W_{max} for (a) case 1, and (b) case 2 at different instants of time mentioned below each arrow in terms of Local Solar Time.

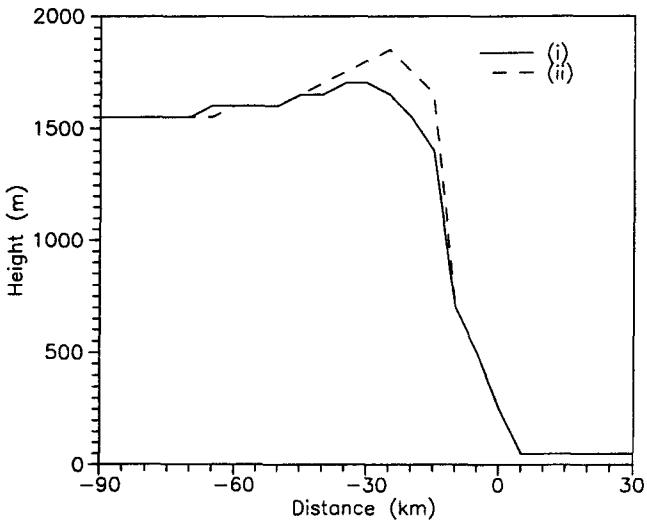

Figure 9. TIBL height at 1400 LST for (i) case 1, and (ii) case 2.

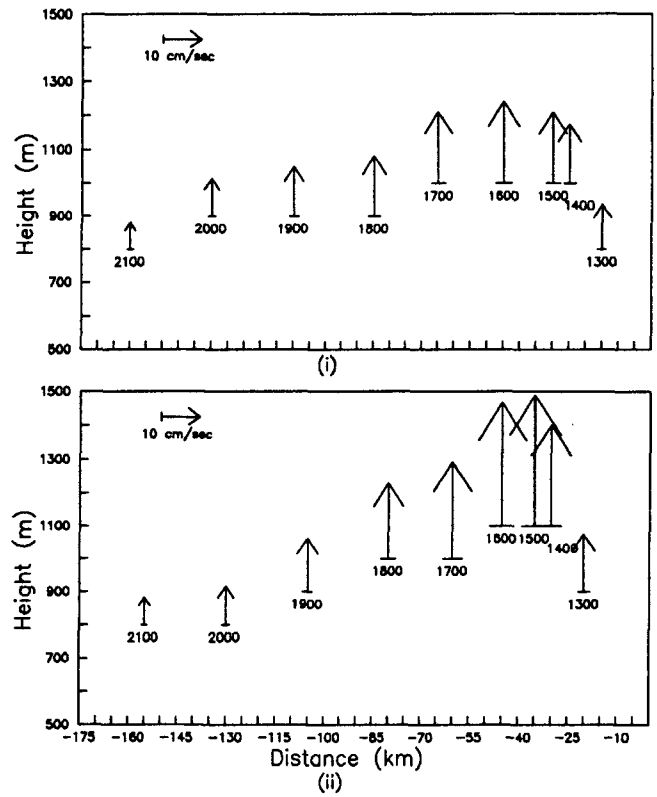

Figure 10. Locations and magnitudes of W_{max} for (i) case 3(a), and (ii) case 3(b) at different instants of time mentioned below each arrow in terms of Local Solar Time.

from 1300 LST for cases 3(a) and (b). Higher values of W_{max} are observed from 1300 to 2000 LST for the case of larger urban width. The value of W_{max} for case 3(a) is 17.6 cm/s and for case 3(b) it is 32.5 cm/s, both occurring at 1500 LST. It is seen from figure 10 that the speed of inland penetration of SBF is not affected much by the variation of urban width. At 1700 LST, SBF for case 3(a) is at 65 km inland while for case 3(b) it is 60 km inland. When the urban width is smaller, SBF takes less time to cross the urban region. In case 3(a), SBF crosses the urban area before 1300 LST and at 1300 LST it is seen at 15 km inland (figure 10(i)). At this time the temperature of the urban area reaches the maximum value of 309.6°K at 10 km inland and the surface temperature contrast between this point and a point in the rural area (80 km inland) is around 0.66°K. At 1400 LST the maximum surface temperature is seen at 30 km inland which is away from the urban region and the surface temperature contrast between this point and the same rural point is 0.4°K (figure 11(i)). In case 3(b) the difference between the surface temperatures of urban (30 km inland) and rural (at 80 km inland) regions is seen to be 1.8°K (309.1°K at the rural point and 310.9°K at the urban point) at 1300 LST and 1.7°K (309.3°K at the rural point and 311.0°K at the urban point) at 1400 LST (figure 11(ii)). Larger surface temperature contrast in case 3(b) causes stronger rural-urban circulation cell as compared to case 3(a), especially during the early afternoon hours. This causes increased convergence and consequent larger W_{max} for the case of larger urban width.

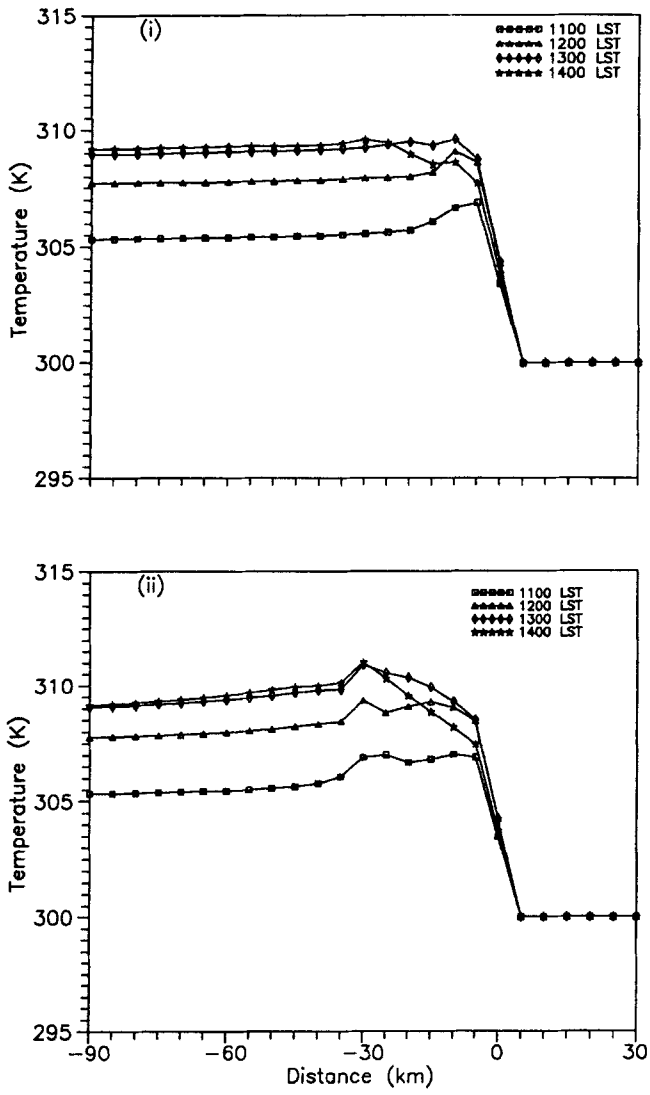

Figure 11. Surface temperature distribution at four instants of time for (i) case 3(a), and (ii) case 3(b).

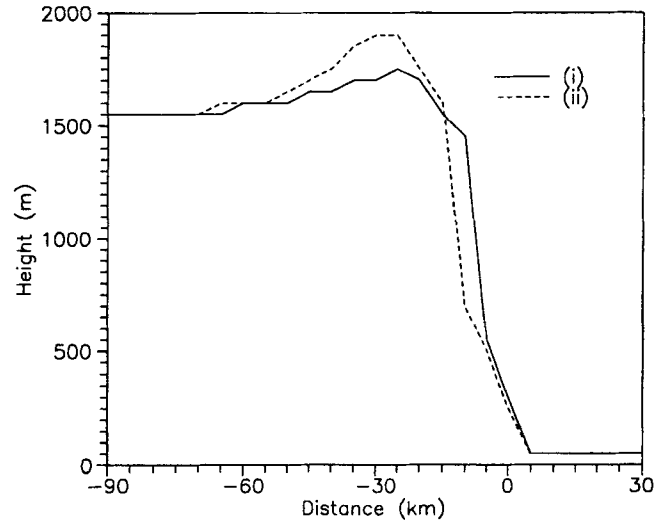

Figure 12. Thermal internal boundary layer height at 1400 LST for (i) case 3(a), and (ii) case 3(b).

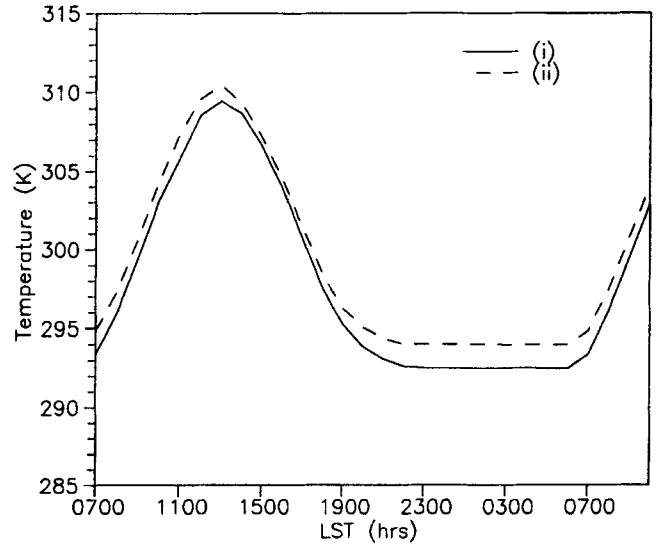

Figure 13. Diurnal surface temperature variation for (i) case 4(a), and (ii) case 4(b).

Figure 12 shows the TIBL height for cases 3(a) and (b) at 1400 LST. In case 3(a) the maximum TIBL height is 1750 m and for case 3(b) it is 1900 m. The higher TIBL in the case of larger urban width can be attributed to stronger heating near the suburban region, increased convergence and increased W_{max} for the case of larger urban width.

3.3 *The effect of change of anthropogenic heat flux*

The effect of anthropogenic heat flux on the diurnal variation of urban surface temperature at 15 km inland is shown in the figure 13. The higher anthropogenic heat flux causes higher urban surface temperature in the morning hours. In the afternoon hours, the advection of cool air from the sea reduces the effect of anthropogenic heat input. Again in the night hours, the effect of anthropogenic heat flux is prominent.

In case 4(a) the weaker heat island intensity induces a very weak and shortlived rural-urban circulation. In this case the maximum speed of rural-urban flow is observed to be 0.45 m/s at 1300 LST. At 1400 LST the rural-urban circulation cell is fully absent. In this case the maximum speed of sea breeze at 1300 LST is 5.08 m/s. In case 4(b), both the speed of sea breeze and rural-urban flow are seen to be higher in the early afternoon. At 1300 LST the maximum speed of sea breeze and that of rural-urban flow are 5.81 m/s and 0.65 m/s, respectively for case 4(b). In case 4(a) the rural-urban circulation cell disappears before 1400 LST, while in case 4(b) it becomes strongest at 1500 LST (0.81 m/s) and persists up to 1700 LST. The existence of rural-urban circulation cell (opposing the sea breeze circulation cell) for a longer time, and the stronger sea breeze circulation in case 4(b) cause stronger convergence and higher W_{max} in the afternoon (figure 14). In case 4(a) the value of W_{max}

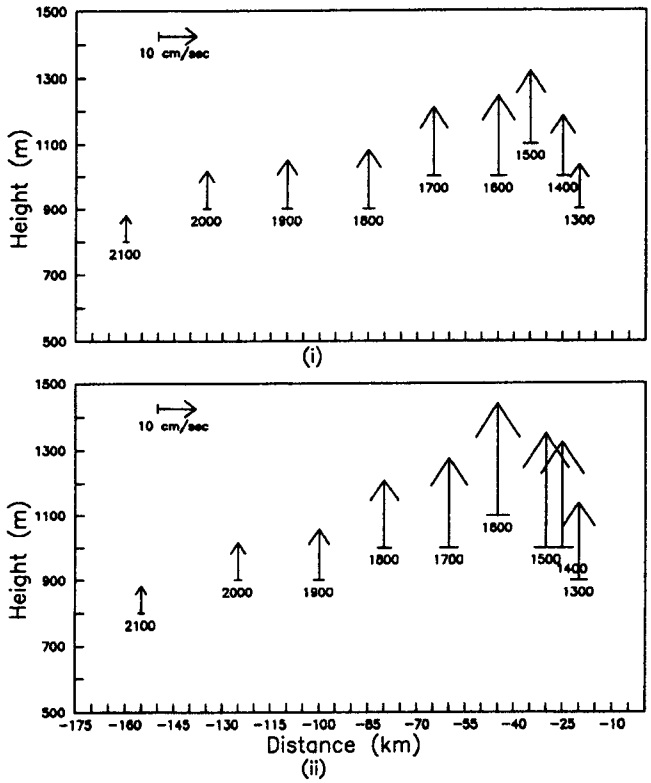

Figure 14. Locations and magnitudes of W_{max} for (i) case 4(a), and (ii) case 4(b) at different instants of time mentioned below each arrow in terms of Local Solar Time.

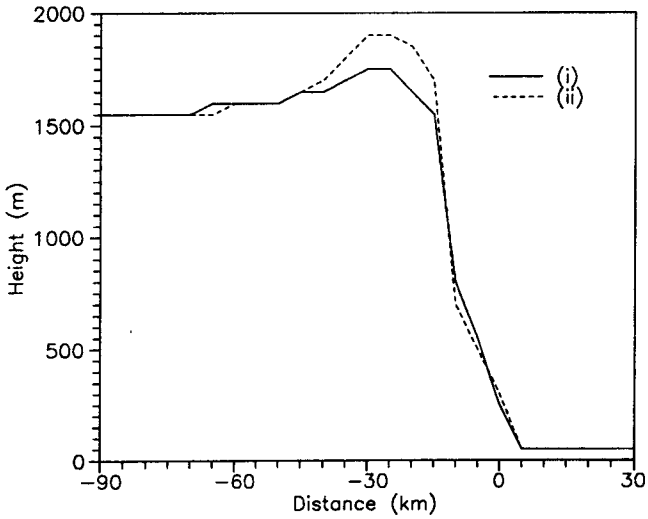

Figure 15. Thermal internal boundary layer height at 1400 LST for (i) case 4(a), and (ii) case 4(b).

obtained at 1500 LST is 18.4 cm/s (figure 14(i)) and that obtained in case 4(b) is 29.5 cm/s (figure 14(ii)).

Figure 15 shows that for the case 4(b), the depth of TIBL is more than that in case 4(a) at 1400 LST in the urban and suburban areas. The maximum TIBL height in case 4(a) at 1400 LST is seen to be 1750 m and that for case 4(b) is 1900 m. The stronger heating and larger ascending motion in this case help the TIBL to grow higher.

4. Summary

The effects of a coastal urban heat island on the sea breeze front and TIBL height in the early afternoon (1400 LST) near the coast are studied by using a two-dimensional numerical mesoscale model. The effects of the growth of the urban heat island on the above features are also studied. The growth of the urban heat island is incorporated in the model by increasing the anthropogenic heat input and the width of the UHI.

In case 1, the sea breeze front and TIBL height are studied without considering the urban area. In case 2, the urban area is considered at the coast. The presence of the urban area causes a weak and shortlived rural-urban circulation in the early afternoon, which opposes the sea breeze front movement and causes reduced inland penetration of the front. Larger values of maximum vertical velocity in the early afternoon hours are obtained in case 2. The TIBL height shows an increase in case 2 over the urban area.

In case 3, the effect of increase of urban width is studied. Increasing the width of the urban area causes increased vertical velocity as well as increased TIBL heights over the urban region.

The effect of the increase of anthropogenic heat input is studied in case 4. The increase of anthropogenic heat input causes increased vertical velocity over the urban area as well as increased TIBL heights.

Acknowledgement

Authors are indebted to Prof. K L Chopra for his encouragement. Many helpful comments of the referees are gratefully acknowledged.

Appendix

u : Horizontal component of momentum along x-axis (ms^{-1}).
v : Horizontal component of momentum along y-axis (ms^{-1}).
w : Vertical component of momentum (ms^{-1}).
θ : Potential temperature (°K).
ϕ : Latitude = $22°N$.
Π : Exner function.
c_p : Specific heat of air at constant pressure ($Jkg^{-1}(°K)^{-1}$).
f : Coriolis parameter (s^{-1}).
K_x : Horizontal eddy exchange coefficient (m^2s^{-1}).
K_z^m : Vertical eddy exchange coefficient for momentum (m^2s^{-1}).
K_z^h : Vertical eddy exchange coefficient for heat ($m^2 s^{-1}$).
g : Gravitational acceleration (ms^{-2}).
R : Gas constant ($Jkg^{-1}(°K)^{-1}$).

z_0 : Roughness length (m).
H : Height of the model top (m).
u_* : Friction velocity (ms^{-1}).
θ_* : Subgrid flux temperature (°K).
q_* : Subgrid flux moisture ($kg\ kg^{-1}$).
p : Pressure (hPa).
p_0 : Reference pressure (hPa).
ρ_s : Soil density $= 2.5 \times 10^3\ kgm^{-3}$.
c_s : Soil specific heat capacity $= 1500\ Jkg^{-1}(°K)^{-1}$.
c_1 : $2\pi^{\frac{1}{2}}$.
c_2 : 2π.
κ_s : Soil thermal diffusivity $= 4.5 \times 10^{-7}\ m^2\ s^{-1}$.
τ_1 : Period of 1 day $= 86400$ s.
A : Albedo $= 0.3$.
S_0 : Solar constant $= 1376\ Wm^{-2}$.
a_f : Fractional absorption $= 0.20$.
T_g : Ground surface temperature (°K).
σ : Stefan Boltzmann constant $= 5.67 \times 10^8\ Wm^{-2}(°K)^{-4}$.
ϵ_s : Emissivity of the ground $= 1.0$.
σ_c : Cloud fraction $= 0$.
q_a : Specific humidity at the anemometer level $= .005\ kgkg^{-1}$.
ρ : Density of air (kgm^{-3}).
L_v : Latent heat of vapourization $= 2262.6 \times 10^3\ Jkg^{-1}$.
q_s : Saturation specific humidity ($kgkg^{-1}$).
T_d : Deep soil temperature $= 295$°K.
T_{av} : Temperature at the anemometer level $= 295$°K.
r_1 : Artificial heat coefficient (Wm^{-2}).
r_2 : Artificial heat coefficient ($Wm^{-2}(°K)^{-1}$).
n : Julian day of the year $= 82$.
Γ : Lapse rate for potential temperature ($°Km^{-1}$).
θ_H : Potential temperature at the model top (°K).
Δt : Time step (s).
θ_{io} : Initial surface potential temperature (°K).
T_m : Temperature close to minimum surface temperature (°K) used in anthropogenic parameterization.

References

Anthes R A 1978 The height of the planetary boundary layer and the production of circulation in a sea breeze model; *J. Atmos. Sci.* **35** 1231–1239

Anthes R A and Warner T T 1978 Development of hydrodynamic models suitable for air pollution and other mesometeorological studies; *Mon. Weather. Rev.* **106** 1045–1078

Arritt R W 1988 Numerical modelling of the offshore extent of sea breezes; *Q. J. R. Meteorol. Soc.* **115** 547–570

Atwater M A 1975 Thermal changes induced by urbanization and pollutants; *J. Appl. Meteorol.* **14** 1061–1071

Atwater M A and Brown P Jr 1974 Numerical calculation of the latitudinal variation of solar radiation for an atmosphere of varying opacity; *J. Appl. Meteorol.* **13** 289–297

Bennett M and Saab A E 1982 Modelling of the urban heat island and of its interaction with pollutant dispersal; *Atmos. Environ.* **16** 1797–1822

Blackadar A K 1978 High resolution models of the planetary boundary layer; *Advances in Environmental and Scientific Engineering.* **1** (Gordon and Breach)

Deardorff J W 1978 Efficient prediction of ground surface temperature and moisture, with inclusion of a layer of vegetation; *J. Geophys.* **83(c4)** 1889–1903

Estoque M A 1961 A theoretical investigation of the sea breeze; *Q. J. R. Meteorol. Soc.* **87** 136–146

Feliks Y 1993 A numerical model for estimation of the diurnal fluctuation of the inversion height due to a sea breeze; *Bound.-Layer Meteorol.* **62** 151–161

Finkele K, Hacker J, Kraus H, Byron-Scott R A D 1995 A complete sea breeze circulation cell derived from aircraft observation; *Bound.-Layer Meteorol.* **73** 299–317

Fisher E L 1961 A theoretical study of the sea breeze; *J. Meteorol.* **18** 215–233

Garratt J R and Physick W L 1985 The inland boundary layer at low latitudes: II sea-breeze influences; *Bound.-Layer Meteorol.* **33** 209–231

Huang C and Sethuraman S 1988 A Numerical modeling study of the marine boundary layer over the gulf stream during cold air advection; *Bound.-Layer Meteorol.* **45** 251–290

Kondo H and Gambo K 1979 The effect of the mixing layer on the sea breeze circulation and the diffusion of pollutants associated with land–sea breezes; *J. Meteorol. Soc. Japan.* **57** 560–575

Kondratyev J 1969 "Radiation in Atmosphere." (New York: Academic Press)

Lu R and Turco R P 1994 Air pollutant transport in a coastal environment. Part I: two-dimensional simulations of sea-breeze and mountain effects; *J. Atmos. Sci.* **51** 2285–2308

Mahrer Y and Pielke R A 1977 The effects of topography on the sea and land breezes in a two-dimensional numerical model; *Mon. Weather. Rev.* **105** 1151–1162

Neumann J and Mahrer Y 1974 A theoretical study of the land and sea breeze circulations; *J. Atmos. Sci.* **28** 532–542

Pielke R A 1974 A three-dimensional numerical model of the sea breezes over South Florida; *Mon. Weather. Rev.* **102** 115–139

Pielke R A 1984 "Mesoscale Meteorological Modeling" (Academic Press)

Physick W L 1980 Numerical experiments on the inland penetration of sea breeze; *Q. J. R. Meteorol. Soc.* **106** 735–746

Seaman N L, Ludwig F L, Donall E G, Warner T T and Bhumralkar C M 1989 Numerical studies of urban planetary boundary-layer structure under realistic synoptic conditions; *J. Appl. Meteorol.* **28** 760–781

Stunder M and Sethuraman S 1985 A comparative evaluation of the coastal internal boundary layer height equations; *Bound.-Layer Meteorol.* **32** 177–204

Vukovich F M, Dunn III J W and Crissman B W 1976 A theoretical study of the St. Louis heat island: the wind and temperature distribution; *J. Appl. Meteorol.* **15** 417–440

Weisman B 1976 On the criteria for the occurrence of fumigation inland from a large lake – A reply; *Atmos. Environ.* **12** 172–173

Xian Z and Pielke R A 1991 The effects of width of landmass on the development of sea breezes; *J. Atmos. Sci.* **30** 1280–1304

Yamamoto G 1975 Generalization of the KEYPS formula in diabatic condition and related discussion on the critical Richardson number; *J. Meteor. Soc. Japan.* **53** 189–194

Yoshikado H 1992 Numerical study of the daytime urban effect and its interaction with the sea breeze; *J. Appl. Meteorol.* **31** 1146–1164

Zhong S and Takle E S 1992 An observational study of sea- and land-breeze circulations in an area of complex coastal heating; *J. Appl. Meteorol.* **31** 1181–1195

MS received 30 March 1995; revised 15 March 1997